Near-Unity Quantum Yields of Biexciton Emission from CdSe/CdS Nanocrystals Measured Using Single-Particle Spectroscopy

Y.-S. Park, A. V. Malko, J. Vela, Y. Chen, Y. Ghosh, F. García-Santamaría, J. A. Hollingsworth, V. I. Klimov, and H. Htoon

Phys. Rev. Lett. **106**, 187401 — Published 3 May 2011

DOI: 10.1103/PhysRevLett.106.187401

Near-Unity Biexciton Emission Quantum Yields in CdSe/CdS Nanocrystals Revealed by Single-Particle Spectroscopy

Y.-S. Park[1,2], A. V. Malko[4], J. Vela[1,2], Y. Chen[1,2], Y. Ghosh[1,2], F. Garcia-Santamaria[1], J. A. Hollingsworth[1,2], V. I. Klimov[1,3*], and H. Htoon[1,2*]

[1]Chemistry Division, [2]Center for Integrated Nanotechnologies and [3]Center for Advanced Solar Photophysics, Los Alamos National Laboratory, Los Alamos, NM 87545, USA

[4]Department of Physics, The University of Texas at Dallas, Richardson, TX 75080, USA

Biexciton photoluminescence (PL) quantum yields (Q_{2X}) of individual CdSe/CdS core/shell nanocrystal quantum dots with various shell thicknesses are derived from independent PL saturation and two-photon correlation measurements. We observe a near-unity Q_{2X} for some nanocrystals with an ultra-thick 19-monolayer shell. High Q_{2X}s are, however, not universal and vary widely among nominally identical nanocrystals indicating a significant dependence of Q_{2X} upon subtle structural differences. Interestingly, our measurements indicate that high Q_{2X}s are not required to achieve complete suppression of PL intensity fluctuations in individual nanocrystals.

PACS numbers: 78.67.Bf, 73.21.La, 78.55.-m

*Corresponding author: htoon@lanl.gov, klimov@lanl.gov

Semiconductor nanocrystal quantum dots (NQDs) with near-perfect photoluminescence (PL) quantum yields (QYs) can be routinely synthesized using methods of colloidal chemistry [1-2]. However, these high QYs can only be obtained for single-exciton (1X) states. QYs of multiexcitons (Q_{mX}, $m > 1$) are, in contrast, very low (<10%) due to fast nonradiative Auger recombination [3-5]. High values of Q_{mX} are, however, essential for practical realization of NQD applications such as lasing [6] and generation of entangled photon pairs [7-8]. To this end, nanorods [9], nanowires [10], and inverted core-shell NQDs [11] have been investigated. They, however, have shown only a moderate suppression of Auger recombination arising primarily from increased spatial separation between carriers. More recently, strongly suppressed Auger decays were reported for alloyed CdZnSe/ZnSe [12] and CdTe/CdSe [13] core/shell NQDs as inferred from observations of reduced blinking [12] and efficient emission from multiexcitons [13] in single-dot studies.

A new type of core/shell NQDs, in which 3-4 nm diameter CdSe cores are overcoated with a thick [>10 monolayers (MLs)] CdS shell, has recently emerged as a promising nanostructure for realizing suppressed Auger recombination [14-15]. Initially, these NQDs (dubbed "giant" or g-NQDs) were reported to exhibit significantly suppressed blinking [14-16]. More recent studies also revealed signatures of suppression of Auger decay including efficient multi-band amplified spontaneous emission [17], long biexciton (2X) recombination times that could not be explained by traditional scaling with NQD volume [17-18], and strong features due to charged excitons (trions) and multiexcitons in single-NQD PL spectra [19-20]. These observations are suggestive of high PL efficiencies of multiexcitons in these structures. However, so far, Q_{mX} in individual g-NQDs have not been measured, neither the uniformity of Q_{mX} across a nanocrystal ensemble has been analyzed.

Here, we address this issue by investigating the distribution of Q_{2X}s in samples of nominally identical g-NQDs using two independent single-dot spectroscopic techniques. We observe excellent agreement between the two methods over a wide range of the Q_{2X} values. We show that Q_{2X} of ~0.9 can be achieved in g-NQDs with shell thickness >16 ML. However, the values of Q_{2X} exhibit a broad distribution indicating a strong influence of NQD internal structure on Q_{2X}. Significantly, even in the case of completely suppressed PL fluctuations (observed for all >16 ML dots), Q_{2X}s and, hence, the degree of Auger decay suppression vary widely. This leads to an important conclusion: the suppression of PL fluctuations and the suppression of Auger decay are not necessarily related. This might imply that the thick shells of our g-NQDs suppress PL fluctuations by either preventing photoionization or restraining random migration of long-lived charges if photoionization still takes place.

CdSe/CdS core/shell NQDs are synthesized via a modified successive ion layer deposition procedure [14]. The NQDs are dispersed on a quartz substrate with the density of ~0.01/ μm^2 and excited with 50 ps, 405 nm laser pulses through a 60X, 0.7 NA objective that is also used to collect PL. The laser repetition rates are selected to ensure complete relaxation of excitons between sequential pulses. The PL spectra are recorded with a cryogenically cooled charge-coupled device through a 1/3 m spectrometer. For two-photon correlation measurements, we use a traditional setup comprising a 50:50 beam splitter and two single-photon Si detectors (350 ps time resolution). All studies are performed at room temperature.

We utilize two independent approaches to measured Q_{mX} in individual NQDs. In the first, we obtain Q_{2X} by analyzing the pump-intensity dependence of the spectrally integrated PL. We assume that upon photoexcitation, the probability of finding an NQD in the N-exciton state is

given by the Poisson distribution: $P(N,\langle N\rangle) = \langle N\rangle^N\, e^{-\langle N\rangle}/N!$, where $\langle N\rangle$ is the average NQD occupancy. This approach requires the knowledge of the NQD absorption cross-section (σ) and certain assumptions on the scaling of the radiative and the nonradiative recombination rates with N. We have also applied an independent method, in which Q_{2X} is derived from the second-order PL intensity correlation ($g^{(2)}$) measurements. This technique, which was recently applied to standard NQDs [21], yields the ratio of the Q_{2X} and single-exciton QY (Q_{1X}) based on the relative amplitudes of the coincidence features in $g^{(2)}$ of the NQD under weak-excitation conditions. This approach is more direct as it does not rely on any of the aforementioned assumptions.

Figure 1(a) displays the pump-power dependence of the spectrally integrated PL of four NQDs with 4, 7, 16 and 19 ML thick CdS shells. For this plot, $\langle N\rangle$ is calculated using σ independently determined by assuming that it scales linearly with the NQD volume [22] (inset of Fig. 1 and Supp. Info). To compare different samples in the same plot, we normalize PL intensities assuming that at low pump levels ($\langle N\rangle < 0.5$) $Q_{1X} = 1$ for all dots. This assumption reduces the number of fitting parameters; the implications of a non-unity Q_{1X} are discussed later in this Letter and also in Supp. Info. While normalized traces are similar at low pump intensities, the PL behavior becomes sample dependent when $\langle N\rangle > 1$ [Fig. 1(a)]. Specifically, normalized PL intensity (I) of the 4- and 7-ML samples reaches complete saturation, while that from the 16- and 19 ML shell dots still grows with $\langle N\rangle$. This increase occurs due to continuing growth of the band-edge PL as well as the development of new higher-energy bands [Figs. 1(b) and 1(c)], indicating enhanced Q_{mX}s values compared to thin-shell samples.

In order to quantitatively describe this behavior, we model I as $I = \sum_{N=1}^{\infty} P(N, \langle N \rangle) \sum_{m=1}^{N} Q_{mX}$. In the case of Q_{mX}(m > 1) = 0, I becomes $I = \left(1 - e^{-\langle N \rangle}\right)$. This saturation curve [solid black line in Fig. 1(a)], which describes a typical behavior of standard dots, falls directly on top of the data points for NQDs with 4- and 7-ML shells. To describe a weak saturation behavior of the 16- and 19-ML shell g-NQDs, we assume that radiative and non-radiative Auger decay rates of the m-exciton state ($k_{mX,R}$ and $k_{mX,NR}$, respectively) scale linearly with the number of available recombination pathways: $k_{mX,R} \propto m^2$ and $k_{mX,NR} \propto m^2(m - 1)$ [23]. Under this assumption, an expression for Q_{mX} can be written as $Q_{mX} = (1 + (m - 1)A)^{-1}$; it contains a single adjustable parameter, $A = k_{2X,NR}/k_{2X,R}$, which defines the value of Q_{2X}: $Q_{2X} = (1 + A)^{-1}$.

We use this model to fit the PL saturation data for 16- and 19-ML shell g-NQDs up to $\langle N \rangle$ of ~25 (Fig. 1a). The fitting provides Q_{2X} of 0.14 ± 0.03 and 0.56 ± 0.04 for the 16- and 19-ML g-NQDs, respectively. At very high pump intensities ($\langle N \rangle > 25$), the PL intensity takes an upward turn, which correlates with the emergence of high-energy emission bands attributed to emission from very high-order mX states [Fig. 1(b) & (c)]. Due to the m^2 and ~m^3 scalings of $k_{mX,R}$ and $k_{mX,NR}$, these states can decay with lifetimes shorter than the pump-pulse width (τ_W ~50 ps) and therefore can recycle more than once [*ca.* $(k_{mX,R} + k_{mX,NR})\tau_W$ times] with a nonzero Q_{mX} within one excitation cycle. The resulting enhancement of the *mX*s' contribution to PL can, in principle, lead to the observed upward turn.

In the second experiment, we extract the Q_{2X}/Q_{1X} ratio from $g^{(2)}(\tau)$ measurements. $g^{(2)}(\tau)$ represents the probability distribution of time intervals between two sequential photon detection events. When one collects only emission from 1X states (e.g., by spectral selection, or in the

cases where *mX* emission is suppressed), $g^{(2)}(\tau)$ exhibits an antibunching behavior for which the area of the $\tau = 0$ peak ($g_0^{(2)}$) is zero. However, $g_0^{(2)}>0$ when the PL signal contains contributions from both 1X and 2X states. In the case of pulsed excitation, $g_0^{(2)}$, which corresponds to the probability of creating 2X and subsequent emission of two photons (2X →1X→0), scales in the lowest order as $\langle N\rangle^2$: $g_0^{(2)} \approx Q_{2X}Q_{1X}\langle N\rangle^2 + O(\langle N\rangle^3)$, where $O(\langle N\rangle^3)$ represents terms with order of $\langle N\rangle^3$ and higher. The area of the side peak measured at $\tau = T$ (*T* is the laser pulse period)($g_s^{(2)}$) that reflects the probability of creation and emission of 1X in two successive excitation events, also scales as $\langle N\rangle^2$: $g_s^{(2)} \approx (Q_{1X}\langle N\rangle)^2 + O(\langle N\rangle^3)$. Due to these scalings, $g_0^{(2)}/g_s^{(2)}$ approaches the value of Q_{2X}/Q_{1X} in the limit of $\langle N\rangle \rightarrow 0$ [24].

The $g^{(2)}$ measurements were conducted on the same individual g-NQDs that were previously investigated using PL saturation. The $g^{(2)}$ traces of the 19 ML dots clearly show the persistence of the zero-delay peak in the $\langle N\rangle \rightarrow 0$ limit [Fig. 2(a)]. Further, the data reveal a clear $\langle N\rangle^2$ scaling of $g_0^{(2)}$ and $g_s^{(2)}$[Fig. 2(b)]. More importantly, as $\langle N\rangle \rightarrow 0$, $g_0^{(2)}/g_s^{(2)}$ approaches 0.18 [Fig. 2(c)], in agreement with $Q_{2X} = 0.22 \pm 0.07$ derived from the PL saturation studies [Fig. 2(c)]. Additional data indicating good agreement between the two approaches are shown in Fig. 3. Well resolvable zero-delay features are found for $g^{(2)}$ traces when $\langle N\rangle < 1$ [Fig. 3(a)-(c)]. As $\langle N\rangle \rightarrow 0$, the $g_0^{(2)}/g_s^{(2)}$ values approach 0.60 (see Supp. Info. for distinguishing single NQDs from NQD clusters), 0.32, and 0.03 in agreement with Q_{2X} of 0.55 ± 0.07, 0.28 ± 0.05 and < 0.05 from the PL saturation analysis. In Fig. 4(a), we plot the Q_{2X} derived from PL saturation studies versus the Q_{2X}/Q_{1X} ratios measured by photon-correlation for 13 NQDs (13 to 19 ML shells).

Grouping of data points around the 45-degree line indicates a near perfect agreement between both measurements.

In our PL saturation analysis, we assumed $Q_{1X} = 1$. In order to understand how the deviation of Q_{1X} from unity affects the accuracy of derived Q_{2X}s, we have simulated 2X QYs for three Q_{1X} values of 0.8, 0.5, and 0.3 and plotted them in Fig 4(a) as a function of $g_0^{(2)}/g_s^{(2)}$, which is assumed to be a true measure of Q_{2X}/Q_{1X}. The simulated data show that while in the regime of low $Q_{2X}/Q_{1X} < 0.3$, the PL saturation approach provides an accurate measure of Q_{2X}/Q_{1X} irrespective of Q_{1X}, a systematic error increases with increasing Q_{2X}/Q_{1X}. However, the fact that the data points for the g-NQDs with the highest Q_{2X}/Q_{1X} ratios are best described by calculations with Q_{1X} of 0.8 to 1 confirms our assumption of Q_{1X} being close to unity.

In Fig. 4(b), we plot a collection of the Q_{2X}s obtained from more than 50 different NQDs via the PL saturation measurement (open data points) and their average values (solid circles) as a function of shell thickness. These results show a consistent increase of Q_{2X} with increasing shell thickness with values for some 19 ML dots approaching a near perfect Q_{2X} of ~0.9. However, we also observe a wide variation of Q_{2X} values ranging from <0.1 to ~0.9 with an average of 0.38 for nominally identical dots. This spread indicates to a wide variation of 2X Auger lifetimes (1.4 - 77.0 ns). Since this large spread is observed for dots with a nominally identical shell thickness, it indicates that factors other than the core and the shell size may also influence Q_{2X}. One such factor is the structure of the core-shell interface affecting the shape of the confinement potential and consequently the rate of Auger recombination as was proposed by Cragg and Efros [24] and studied experimentally by García-Santamaría et al. [18].

The observed wide variation in 2X Auger time constants further suggests the existence of similarly wide variation of lifetimes of charged exciton (trions) because they are dependent on the same Auger process. Since the trions have been often invoked in various PL blinking models of standard NQDs [25-26], one might expect that the observed spread in the degree of Auger decay suppression could have effect on PL fluctuation behaviors in g-NQDs. However, our studies of PL time trajectories of more than 40 thick-shell (16 and 19 ML) dots show that all of them exhibit blinking-free PL (with nearly shot-noise limited photon-count-rate fluctuations independent of pump fluence) despite a wide variation in the Q_{2X} values (Supp. Info Fig. S6). This observation suggests that the suppression of Auger recombination, which is required to obtain high QYs for 2X as well as trions, is not necessary to achieve complete suppression of PL intensity fluctuations. This further implies that blinking suppression in g-NQDs results most likely from either suppression of photoionization or inhibition of random migration of long-lived charges generated by photoionization.

To summarize, we have studied Q_{2X}s in individual g-NQDs via two independent approaches and the results from both techniques are in excellent agreement. Our experiments reveal that it is possible to achieve a near-unity Q_{2X} in thick-shell g-NQDs. For all samples, we observe significant dot-to-dot variations in Q_{2X}, which indicates that besides simple "geometric" factors (e.g., the core and the shell sizes), mX QYs strongly depend on more subtle structural features such as an internal shell structure and/or the properties of the core/shell interface. We also observe that suppression of PL intensity fluctuations in g-NQDs does *not* require the suppression of Auger recombination suggesting that a fluctuation-free behavior of PL in thick-shell CdSe/CdS g-NQDs likely results from either suppression of photoionization or inhibition of random migration of long-lived charges if photoionization still takes place.

This work was conducted, in part, at the Center for Integrated Nanotechnologies (CINT), a U.S. Department of Energy, Office of Basic Energy Sciences (OBES) user facility. We acknowledge D. Werder for performing transmission electron microscopy studies. Y.P. is supported by CINT. Y.G., J.V., Y.C. acknowledge Los Alamos National Laboratory Directed Research and Development Funds. Work of A.V.M was supported by UT Dallas start-up funds. V.I.K. is supported by the Center for Advanced Solar Photophysics, an Energy Frontier Research Center of the OBES, Office of Science (OS), U.S. DOE. F.G. is supported by the Chemical Sciences, Biosciences and Geosciences Division of OBES, U.S. DOE. H.H. and J.A.H. acknowledge a Single-Investigator Small-Group Research Award (2009LANL1096), OBES, OS, U.S. DOE.

[1] R. Xie *et al.*, J. Am. Chem. Soc. **127**, 7480 (2005).

[2] J. McBride *et al.*, Nano Lett. **6**, 1496 (2006).

[3] B. Fisher *et al.*, Phys. Rev. Lett. **94**, 087403 (2005).

[4] V. I. Klimov *et al.*, Science **287**, 1011 (2000).

[5] L.-W. Wang *et al.*, Phys. Rev. Lett. **91, 056404** (2003).

[6] V. I. Klimov *et al.*, Science **290**, 314 (2000).

[7] A. Muller *et al.*, Phys. Rev. Lett. **103**, 217402 (2009).

[8] R. M. Stevenson *et al.*, Nature **439**, 179 (2006).

[9] H. Htoon *et al.*, Phys. Rev. Lett. **91**, 227401 (2003).

[10] I. Robel *et al.*, Nano Lett. **6**, 1344 (2006).

[11] J. Nanda *et al.*, J. App. Phys. **99**, 034309 (2006).

[12] X. Wang *et al.*, Nature **459**, 686 (2009).

[13] R. Osovsky *et al.*, Phys. Rev. Lett. **102**, 197401 (2009).

[14] Y. Chen *et al.*, J. Am. Chem. Soc. **130**, 5026 (2008).

[15] B. Mahler *et al.*, Nat. Mater. **7**, 659 (2008).

[16] J. Vela *et al.*, J. Biophotonics **3**, 706 (2010).

[17] F. García-Santamaría *et al.*, Nano Lett. **9**, 3482 (2009).

[18] F. García-Santamaría *et al.*, Nano Lett. **11**, 687 (2011).

[19] P. Spinicelli *et al.*, Phys. Rev. Lett. **102**, 136801 (2009).

[20] H. Htoon *et al.*, Nano Lett. **10**, 2401 (2010).

[21] G. Nair, J. Zhao, and M. G. Bawendi, Nano Lett., 10.1021/nl104054t (2011).

[22] V. I. Klimov, J. Phys. Chem. B **104**, 6112 (2000).

[23] J. A. McGuire *et al.*, Acc. Chem. Res. **41**, 1810 (2008).

[24] G. E. Cragg, and A. L. Efros, Nano Lett. **10**, 313 (2010).

[25] A. L. Efros, and M. Rosen, Phys. Rev. Lett. **78**, 1110 (1997).

[26] K. Zhang *et al.*, Nano Letters **6**, 843 (2006).

Figure Captions

FIG. 1. (Color online) (a) Pump-power dependence of the PL intensity for four single NQDs. Solid lines are the fits to the "PL-saturation" model which yields $Q_{2X} \approx 0.14$ and 0.56 for 16- and 19-ML shell NQDs, respectively. Inset: NQD absorption cross-sections plotted as a function of shell thickness. Pump-power-dependent PL spectra of (b) 16- and (c)19-ML shell g-NQDs showing the emergence of higher-energy emission bands (575-450 nm) at large $\langle N \rangle$.

FIG. 2. (Color online) (a). The $g^{(2)}$ measurements for a single 19-ML shell g-NQD at different pump intensities. The zero-delay signal still persists at $\langle N \rangle < 1$. (b) Total PL (Δ) and time-integrated areas of $g_0^{(2)}$ (□) and $g_s^{(2)}$(○) plotted as a function of $\langle N \rangle$. (c) Plot of $g_0^{(2)}/g_s^{(2)}$vs. $\langle N \rangle$(dotted line) approaches 0.18 as $\langle N \rangle \rightarrow 0$, in agreement with $Q_{2X} = 0.22 \pm 0.07$ obtained from the PL saturation analysis (dotted lines in b).

FIG. 3. (Color online) (a)- (c) $g^{(2)}$ traces measured at $\langle N \rangle = 0.46$, 0.34, and 1 for NQD 1, 2 and 3, respectively . NQD1 and NQD2 have the shell thickness of 19 MLs and NQD3 has a 16-ML-thick shell. (d) The plot of $g_0^{(2)}/g_s^{(2)}$ vs. $\langle N \rangle$ gives $g_0^{(2)}/g_s^{(2)}$of 0.60 (NQD1), 0.32 (NQD2) and 0.03 (NQD3) as the $\langle N \rangle \rightarrow 0$. (e) The PL intensity saturation analysis for the same set of the NQDs yields Q_{2X} of 0.55 ± 0.07, 0.28 ± 0.05 and <0.05, respectively.

FIG. 4. (Color online) (a) A plot of the Q_{2X} vs. Q_{2X}/Q_{1X} for 13 different single g-NQDs. Solid, dashed, dotted and dashed-and-dotted traces represent the simulations of Q_{2X} for the "PL-saturation" model for Q_{1X} of 1.0, 0.8, 0.5 and 0.3, respectively. (b) Q_{2X} obtained from the "PL-

saturation" model for >50 individual NQDs (open symbols); average Q_{2X} for a given shell thickness are shown by solid circles.

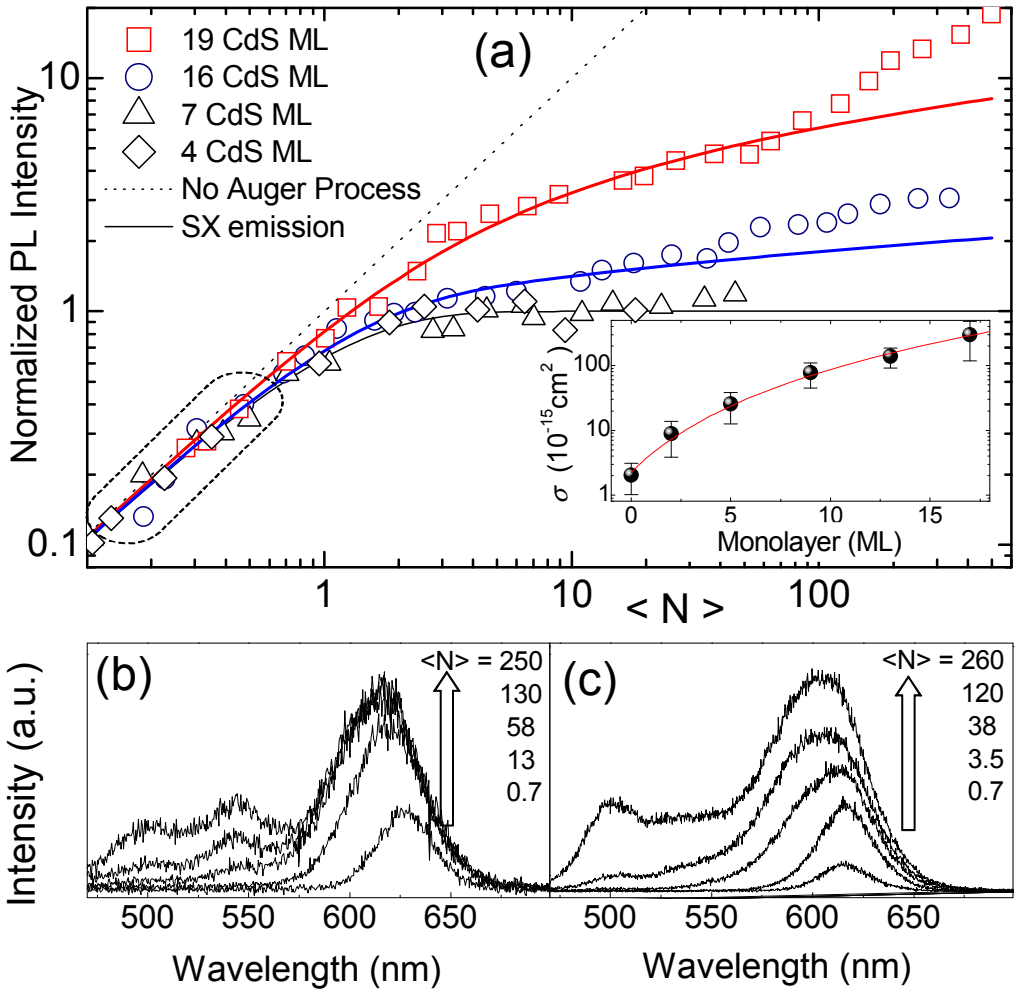

Figure 1, Y.-S. Park et al.,
Submitted to Phys. Rev. Lett.
Actual size: Width: 3.4": Height: 3.0"

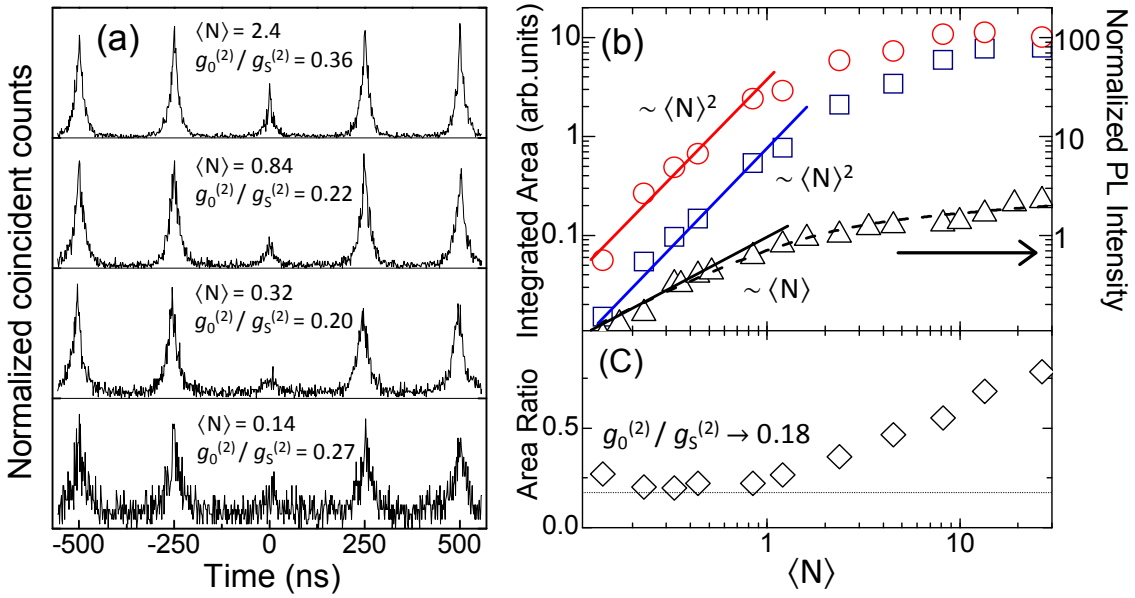

Figure 2, Y.-S. Park et al.,
Submitted to Phys. Rev. Lett.
Actual size: Width: 3.4": Height: 1.9"

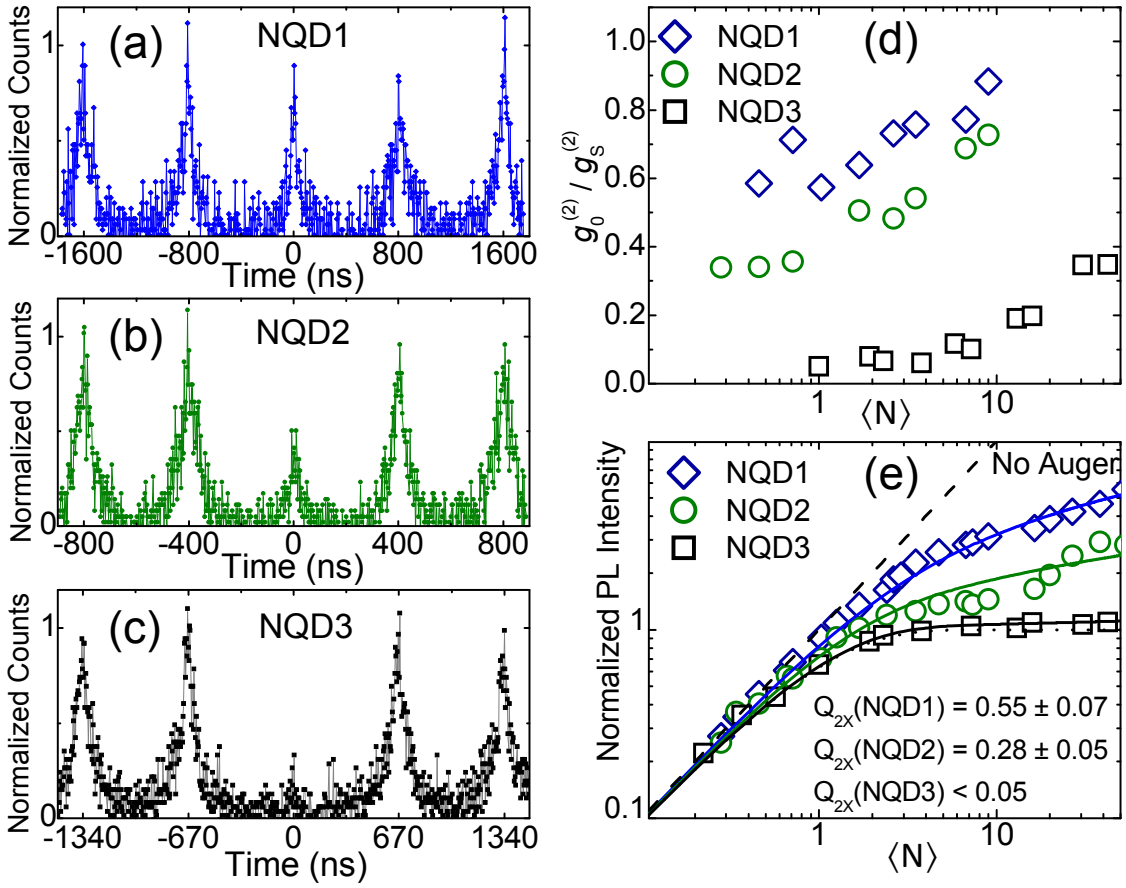

Figure 3, Y.-S. Park et al.,
Actual size: Width: 3.4": Height: 2.69"
Submitted to Phys. Rev. Lett.

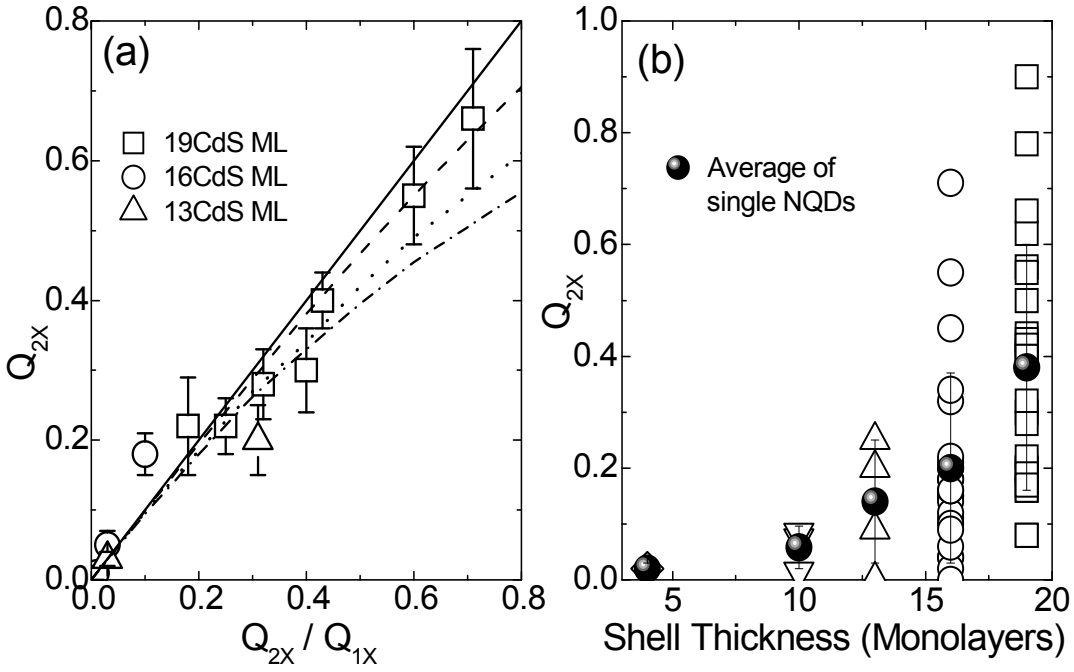

Figure 4, Y.-S. Park et al.,

Actual size: Width: 3.4": Height: 2.1"
Submitted to Phys. Rev. Lett.